Tanzania Journal of Science
Volume 51(4), 2025
journal homepage: https://commons.udsm.ac.tz/tjs/

The analysis of non-Newtonian blood flow through an atherosclerotic artery in the presence of body acceleration, radiation effect and magnetic field

Johnson N Katabwa[1*] and Makungu J Ng'oga[2]
[1] *Department of Management studies, Tanzania Institute of Accountancy*
P.O.Box 5247, Mwanza, Tanzania
[2] *Department of Mathematics, University of Dar-es-Salaam, P.O. Box 35062, Dar es Salaam, Tanzania*

Keywords

Non-Newtonian;
Atherosclerotic Artery;
Herschel-Bulkley Fluid Model;
Radiation Effect;
Magnetic Field;
Body Acceleration

Abstract

The unsteady analysis of two-dimensional laminar flow of the non-Newtonian blood through an atherosclerotic artery in the presence of body acceleration, radiation effect and magnetic field has been studied. The blood flow has been assumed to satisfy the Herschel-Bulkley fluid model characteristics. The two-dimensional model equations have been developed from the physical laws of continuity, momentum and energy conservation. These equations are transformed to non-dimensional form and solved numerically using explicit finite difference method under suitable radial coordinate transformation. The study findings show that, the presence of body acceleration increases both velocity and temperature profiles of the blood in the artery while the influence of applied magnetic field reduces the velocity of blood. It is also noticed that the effect of thermal radiation within the stenosed arterial segment leads to an increase in the local blood temperature through the radiative process.

Introduction

In the recent years, many cardiovascular diseases particularly atherosclerosis or medically called stenosis have been found to be the major cause of many deaths of people worldwide, especially in low-and middle-income countries (WHO, 2025). These diseases result from narrowing of human arterial system due to the accumulation of fats, cholesterols and other lipid deposits in the arterial walls which collectively form plaque. The continued formation of plaque in arterial walls reduces the normal flexibility in blood transportation and as it extends more may lead to the other cardiac diseases such as heart failure, myocardial infarction and cerebral strokes (Issah et al. 2024). These atherosclerotic conditions are mostly inhabited in Carotid arteries which supply blood to brain and coronary arteries which supplies blood to heart muscles. Therefore, the modelling of blood flow in atherosclerotic arteries has been attracting the interests from different mathematicians and modelers to work on due to their significant applications in health and medical fields.

Blood as it flows from the heart to various organs of the body via different vessel routes can be categorized as a Newtonian or non-Newtonian fluid. A non-Newtonian fluid is the one which exhibits the non-linear relationship between its shear stress and rate of strain. By the study of Sochi (2013) blood can be assumed to be Newtonian fluid when flows in large blood vessels such as ventricles, arteries and veins under medium to high shear rates. However, at low shear rates the flow within narrow vessels, e.g. capillaries and coronary arteries, the blood is assumed to be a non-Newtonian fluid. The impact of the non-Newtonian character can be described by a number of factors such as pathological blood rheology and flow in stenosed tube, (Huang et al. 2013).

The abnormal flow of blood may happen whenever human body is subjected to changes in external accelerations. This occurs if a person performs extensive physical exercises such as running, riding bicycle and others. According to Tanwar et al. (2016) model, the influence of body acceleration force causes unusual changes on the blood flow characteristics which may mimic serious physical disorders such as loss of vision, increase of pulse rates and abdominal pains of the body. Aziz et al. (2023), presented a theoretical model on the analysis of pulsatile blood flow through elliptical multi-stenosed inclined artery influenced by body acceleration. They revealed that the effect of yield stress and stenosis reduce the blood flow rate whereas the influence of body acceleration increases the flow of blood.

Additionally, the context of radiation effect is related to any mechanism that induces thermal energy in the blood flow system. This can occur as a result of metabolic activities in body tissues such as inflammation, presence of excessive heat environments around the human body and applied thermotherapy in clinical treatments of injured patients. It was revealed from the findings of Lilian et al. (2023), that the viscous energy dissipation in arterial walls due to arterial stiffness can enhance storage of heat in blood which significantly increases its

[*]*Corresponding author email: johnson.katabwa@tia.ac.tz*
Received 1 May 2025; Revised 08 Dec 2025; Accepted 12 December 2025; Published 30 December 2025
https://doi.org/10.65085/2507-7961.1120

ISSN 0856-1761, e-ISSN 2507-7961

temperature. The variation of the generated heat may cause changes on blood velocity, vessel diameter, temperature of the surrounding tissues and heat transfer coefficient of blood. Sinha et al. (2016), observed that brain can share 16% of the total heat generated in the whole body while about two-thirds of total heat generated in the body at rest is due to metabolic activities in the thorax, the abdomen and the brain. Gupta et al. (2013) investigated on Modelling of hyperthermia-induced temperature distribution and explored that blood flow system is whole affected by thermal response of living tissues. Also, the application of heat source and chemical reaction in MHD blood flow through permeable bifurcated arteries with inclined magnetic field in tumor treatments was studied by Devendra et al. (2021). Meanwhile, Amos et al. (2022) studied on chemical reaction, heat source and slip effects on MHD blood flow in stenosed artery under body acceleration and revealed that the presence of heat source and body acceleration enhance blood flow rate whereas magnetic field and chemical reaction decrease blood flow rate. In their findings Prakash and Makinde (2011) on radiative heat transfer to blood flow through a stenotic artery in the presence of magnetic field showed that, the patients undergoing thermal radiation therapy have an advantage of reducing the resistance of blood flow in the affected arteries by increased thermal radiation absorption.

Furthermore, applying external magnetic field intensity on the body also brings significant changes on blood flow system. By treating blood to obey a power law fluid model, Varshiney et al. (2010) conducted a numerical study on the effects of external applied magnetic field on arteries having multiple stenoses. The findings indicate that blood flow characteristics are significantly influenced by the presence of multiple stenoses and the externally applied magnetic field of varying intensities.

The findings of Mwapinga et al. (2020), on non-Newtonian heat and mass transfer on MHD pulsatile flow of blood through stenosed artery in the presence of body acceleration postulated that the increase of body acceleration enhances velocity of the blood while the external applied magnetic field reduces the blood flow rate.

The general objective of this study is to conduct a comprehensive analysis of non-Newtonian blood flow through a stenosed artery, highlighting the combined effects of body acceleration, thermal radiation and an applied magnetic field. To the best of our knowledge the simultaneous influence of these three factors; i.e, body acceleration force, radiation effects and magnetic fields within a single thermodynamic model has not been widely done in prior research. Specifically, the study aims to explore the role of radiation on blood circulation across different temperature profiles and to analyze the impact of body acceleration and magnetohydrodynamic (MHD) effects on the thermodynamic stability of blood flow under varying atherosclerotic conditions. The findings of this research will contribute deeper understanding of blood flow dynamics in affected arteries under complex physiological factors. Furthermore, the study has potential clinical implications by supporting biomedical scientists and clinicians in the management of cardiovascular diseases. It offers insights that could improve the application of therapeutic techniques such as magnetotherapy and thermotherapy, thus enhancing blood circulation and treatment outcomes for patients affected by atherosclerosis

Mathematical Formulation

The analysis of unsteady two-dimensional laminar flow of blood in non-porous atherosclerotic artery in the presence of body acceleration, radiation effect and magnetic field is studied. The study assumes that the blood flow is unsteady, incompressible, axisymmetric and satisfies Herschel-Bulkley fluid model. The body acceleration force $G(t)$ is imposed along the flow and the external magnetic field strength B_0 is applied perpendicular to the flow. In addition, it is considered that the cylindrical coordinate systems of an artery are, (r, θ, z) representing the radial, tangential and axial blood flow axes while R being the radius of an artery in a normal region. Moreover, $h(z)$ is the geometry of the stenosed region of an artery which depends onz_0 meanwhile, $2z_0$, δ and L stands for length of stenosed region of an artery, protuberance of stenosis and the length of the whole arterial system as represented in the diagram below.

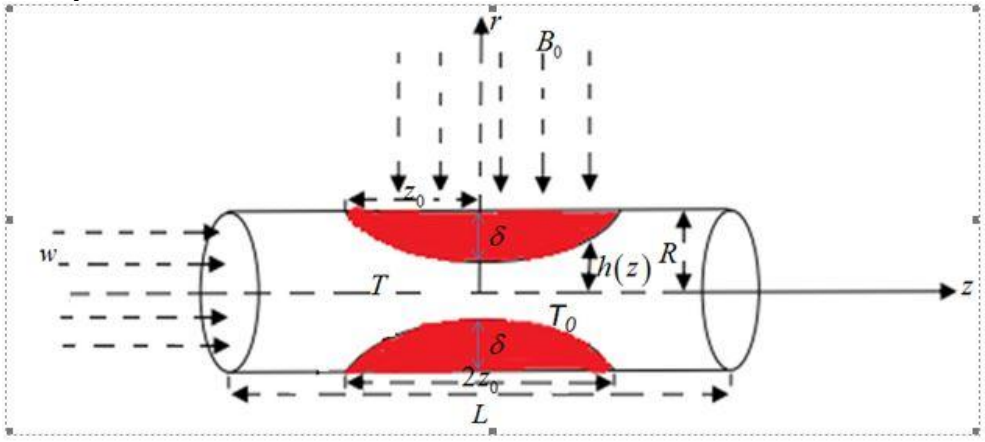

Figure 1: A Schematic flow diagram of an atherosclerotic artery.

Therefore, basing on the Boussinesq approximation, the two-dimensional model equations of continuity, momentum and energy conservation are:

$$\frac{\partial u}{\partial r}+\frac{u}{r}+\frac{\partial w}{\partial z}=0 \tag{1}$$

$$\rho\left(\frac{\partial u}{\partial t}+u\frac{\partial u}{\partial r}+w\frac{\partial u}{\partial z}\right)=-\frac{\partial p}{\partial r}+\frac{1}{r}\frac{\partial(r\tau_{rr})}{\partial r}+\frac{\partial(\tau_{rz})}{\partial z} \tag{2}$$

$$\rho\left(\frac{\partial w}{\partial t}+u\frac{\partial w}{\partial r}+w\frac{\partial w}{\partial z}\right)=-\frac{\partial p}{\partial z}+\frac{1}{r}\frac{\partial(r\tau_{zr})}{\partial r}+\frac{\partial(\tau_{zz})}{\partial z}+G(t)-\sigma B_0^2 w \tag{3}$$

$$\mathbf{\rho C_p}\left(\mathbf{\frac{\partial T}{\partial t}+u\frac{\partial T}{\partial r}+w\frac{\partial T}{\partial z}}\right)=\mathbf{k}\left(\mathbf{\frac{\partial^2 T}{\partial r^2}+\frac{1}{r}\frac{\partial T}{\partial r}+\frac{\partial^2 T}{\partial z^2}}\right)+\mathbf{q_r(T-T_0)}+\mathbf{\tau_{rr}\frac{\partial u}{\partial r}+\tau_{zz}\frac{\partial w}{\partial z}+\tau_{rz}\left(\frac{\partial w}{\partial r}+\frac{\partial u}{\partial z}\right)} \tag{4}$$

Following Das and Saha (2009), the geometry of an atherosclerotic artery in figure 1, is mathematically defined as:

$$h(z)=\begin{cases}R-\delta\left(1+cos\frac{\pi z}{z_o}\right); -z_o\le z\le z_o\\ R \qquad \text{otherwise}\end{cases} \tag{5}$$

In equations (1) - (4), *u, w,* and σ are radial velocity, axial velocity, and the electrical conductivity of blood, respectively. Moreover, C_p and k represent the specific heat capacity of blood at the constant pressure, and thermal conductivity constant of blood respectively, whileq_r being the quantity of radiant heat in the arterial system. Furthermore, the difference in temperature $T-T_o$ in the arterial system makes a possible occurrence of thermal radiation around a stenosed region of an artery as supported by (Sharma and Gaur, 2018). Moreover, τ_{rr} and τ_{zz} represent the normal stress components acting perpendicular to the flow whereas τ_{rz} is the shear stress component in the arterial wall. The study assumes the blood to satisfy the Herschel-Bulkley fluid model, so the stresses on arterial wall are defined by the equation below:

$$\boldsymbol{\tau_{ij}}=\begin{cases}\left(\tau_0\dot{\Upsilon}^{-1}+\mathrm{K}\dot{\Upsilon}^{\boldsymbol{n-1}}\right)\dot{\Upsilon}_{ij} & \text{for} \quad \tau\ge\tau_0\\ \dot{\Upsilon}=0 & \text{for} \quad \tau<\tau_0\end{cases} \tag{6}$$

Where, $\boldsymbol{\tau_{ij}}$ represent the extra stress tensor components for which $\boldsymbol{(i,j)=(r,z)}$ directions, $\boldsymbol{K}$ is the blood consistency index, $\boldsymbol{n}$ is the flow index of blood and $\boldsymbol{\tau_0}$ is the yield stress value at shear rate zero.

$\dot{\boldsymbol{\Upsilon}}$ represents, the magnitude of shear rate and its expression is:

$$\dot{\Upsilon}=\left[2\left(\left(\frac{\partial u}{\partial r}\right)^2+\left(\frac{u}{r}\right)^2+\left(\frac{\partial w}{\partial z}\right)^2\right)+\left(\frac{\partial u}{\partial z}+\frac{\partial w}{\partial r}\right)^2\right]^{1/2} \tag{7}$$

Therefore, from equation (6) the normal and shear stresses of blood τ_{rr} , τ_{zz} and τ_{rz} along r and z directions are computed by:

$$\begin{cases}\tau_{rr}=2\left(\tau_0\dot{\Upsilon}^{-1}+\mathrm{K}\dot{\Upsilon}^{\boldsymbol{n-1}}\right)\frac{\partial u}{\partial r}\\ \tau_{rz}=\left(\tau_0\dot{\Upsilon}^{-1}+\mathrm{K}\dot{\Upsilon}^{\boldsymbol{n-1}}\right)\left(\frac{\partial u}{\partial z}+\frac{\partial w}{\partial r}\right)\\ \tau_{zz}=2\left(\tau_0\dot{\Upsilon}^{-1}+\mathrm{K}\dot{\Upsilon}^{\boldsymbol{n-1}}\right)\frac{\partial w}{\partial z}\end{cases} \tag{8}$$

The pressure gradient along radial flow is assumed to be very minimal due to the reduced lumen of an artery compared to the increase of pressure waves, implying that: $\frac{\partial p}{\partial r}\approx 0$. This assumption reflects the dominance of axial flow and negligible radial pressure variations under normal physiological conditions. However, it is possible that in cases of significant vasodilation or vasoconstriction, especially in smaller or highly reactive vessels, radial pressure gradients may become non-negligible due to altered wall compliance and flow behavior. Therefore, the study assumes the condition $\frac{\partial p}{\partial r}\approx 0$ holds and hence pressure gradient leading the pulsatile flow of blood in the axial direction is defined as: $\frac{-\partial p}{\partial z}=A_0+A_1cos(\omega t), t\ge 0$. Whereas, $A_0 is$the steady amplitude of the pressure gradient, A_1 is the amplitude of the pulsatile flow and $\omega=2\pi f_p$, where f_p is a heart pulse frequency. The lumen diameter interacts with pulse frequency by influencing wave propagation and flow resistance. The change in pulse frequency brings the variations in heart rates which significantly affect flow dynamics, especially in vessels with compliant walls or variable geometry. Apart from this body acceleration force is defined by: $G(t)=\rho a_0 cos(\omega_1 t+\phi), t\ge 0$ for whichρa_0 represents the amplitude of body acceleration and a_0 is the body acceleration parameter, $\omega_1=2\pi f_0$where $f_0$is the body acceleration frequency, ϕ is the phase difference angle.

Boundary and initial conditions

At $\boldsymbol{t=0}$ it is assumed that model equations (1) - (4) hold the conditions:

$$u(r,z,0)=u_0, \quad w(r,z,0)=w_0 \quad \text{and} \quad T(r,z,0)=T_0 \tag{9}$$

While the boundary conditions are:

$$u(r,z,t) = w(r,z,t) = 0,\ T(z,r,t) = T_w \quad \text{at } r = h(z) \tag{10}$$

$$\frac{\partial w(r,z,t)}{\partial r} = \mathbf{0}, \frac{\partial T(r,z,t)}{\partial r} = \mathbf{0}, \boldsymbol{u(r,z,t) = 0} \ \text{ at } \boldsymbol{r = 0} \tag{11}$$

Non-Dimensionalization of the Model Equations

The non-dimensional model quantities are introduced in this section and for convenience we let $\boldsymbol{u_c}$ to be the characteristic velocity of the blood and R is the radius of the normal artery. Therefore, the dimensionless variables are as follows:

$$\eta = \frac{r}{R}, \quad w^* = \frac{w}{u_c}, \ u^* = \frac{u}{u_c}, \quad t^* = \frac{tu_c}{R}, \quad z^* = \frac{z}{z_o} \quad p^* = \frac{p}{\rho u_c^2} \tag{12}$$

$$A_0{}^* = \frac{A_0 R}{\rho u_c^2}, \ A_1{}^* = \frac{A_1 R}{\rho u_c^2}, \quad \omega^* = \frac{R\omega}{u_c}, \quad \omega_1{}^* = \frac{R\omega_1}{u_c}, a_0{}^* = \frac{R\, a_0}{u_c^2} \quad e = \frac{\delta}{R} \tag{13}$$

$$\tau_{ij}{}^* = \frac{\tau_{ij}}{\rho u_c^2}\ , \ \boldsymbol{\tau_o}{}^* = \frac{\boldsymbol{\tau_o}}{\boldsymbol{\rho u_c^2}}, T_w{}^* = \frac{T_w - T_0}{T_0}, \quad T_o{}^* = \frac{T_0}{T_w}\ , \ h^*(z^*) = \frac{h(z)}{R} \tag{14}$$

For the aim of mathematical simplification, the asterisks are dropped when substituting equations (12) - (14) into equations (1) - (5) to obtain the dimensionless model equations of the simplified version as shown hereunder:

$$\frac{\partial \mathrm{u}}{\partial \eta} + \frac{\mathrm{u}}{\eta} + \frac{\partial \mathrm{w}}{\partial \mathrm{z}} = 0 \tag{15}$$

$$\frac{\partial u}{\partial t} + u\frac{\partial u}{\partial \eta} + w\frac{\partial u}{\partial z} = \frac{1}{\eta}\frac{\partial(\eta\tau_{rr})}{\partial \eta} + \frac{\partial(\tau_{rz})}{\partial z} \tag{16}$$

$$\boldsymbol{\frac{\partial w}{\partial t} + u\frac{\partial w}{\partial \eta} + w\frac{\partial w}{\partial z} = A_0 + A_1 cos(\omega t) + \frac{1}{\eta}\frac{\partial(\eta\tau_{rz})}{\partial \eta} + \frac{\partial(\tau_{zz})}{\partial z} + a_0\cos(\omega_1 t + \phi) - \frac{Ha^2}{Re}w.} \tag{17}$$

$$\frac{\partial T}{\partial t} + u\frac{\partial T}{\partial \eta} + w\frac{\partial T}{\partial z} = \frac{1}{Pr}\left(\frac{\partial^2 T}{\partial \eta^2} + \frac{1}{\eta}\frac{\partial T}{\partial \eta} + \frac{\partial^2 T}{\partial z^2}\right) + Ec\begin{bmatrix}\tau_{rr}\frac{\partial u}{\partial \eta} + \tau_{zz}\frac{\partial w}{\partial z} + \\ \tau_{rz}\left(\frac{\partial w}{\partial \eta} + \frac{\partial u}{\partial z}\right)\end{bmatrix} + RdT \tag{18}$$

Where; $\boldsymbol{Re} = \frac{R^n\rho}{Ku_c^{n-2}}$, $\boldsymbol{Ha} = \boldsymbol{B_0}\left(\frac{\sigma R^{n+1}}{Ku_c^{n-1}}\right)^{\frac{1}{2}}$, $\boldsymbol{Pr} = \frac{\rho u_c R C_p}{k}$, $\boldsymbol{Ec} = \frac{u_c^2}{C_p(T_w - T_0)}$ and $\boldsymbol{Rd} = \frac{q_r R^2}{\rho u_c R C_p}$ are generalized Reynolds' number, Hartmann number, Prandtl number, Eckert number and Radiation parameter source respectively.

The dimensionless stress tensor components are defined as:

$$\boldsymbol{\tau_{ij}} = \begin{cases}\left(\frac{1}{Re}\dot{\Upsilon}^{n-1} + \tau_0\dot{\Upsilon}^{-1}\right)\dot{\Upsilon}_{ij} \\ \dot{\Upsilon} = 0 \quad \text{for} \quad \tau < \tau_0\end{cases} \tag{19}$$

With:

$$\dot{\Upsilon} = \sqrt{2\left[\left(\frac{\partial u}{\partial \eta}\right)^2 + \left(\frac{u}{\eta}\right)^2 + \left(\frac{\partial w}{\partial z}\right)^2\right] + \left(\frac{\partial u}{\partial z} + \frac{\partial w}{\partial \eta}\right)^2} \tag{20}$$

And also;

$$\tau_{rr} = 2\left(\frac{1}{Re}\dot{\Upsilon}^{n-1} + \tau_0\dot{\Upsilon}^{-1}\right)\frac{\partial u}{\partial \eta} \tag{21}$$

$$\tau_{zz} = 2\left(\frac{1}{Re}\dot{\Upsilon}^{n-1} + \tau_0\dot{\Upsilon}^{-1}\right)\frac{\partial w}{\partial z} \tag{22}$$

$$\tau_{rz} = \left(\frac{1}{Re}\dot{\Upsilon}^{n-1} + \tau_0\dot{\Upsilon}^{-1}\right)\left(\frac{\partial u}{\partial z} + \frac{\partial w}{\partial \eta}\right) \tag{23}$$

The dimensionless initial and boundary conditions are:

$w_0 = \left(\frac{A_0 + A_1}{4}\right)(1 - \eta^2)$, this is the initial velocity along axial flow at steady state. This form satisfies the no-slip condition at the arterial wall ($\eta = 1$), and imply that velocity is maximum at the centerline ($\eta = 0$). This is consistent initial condition for the pulsatile flow evolution governed by the time-dependent pressure gradient.

$$u(\eta, z, 0) = 0 \text{ and } \quad T(\eta, z, 0) = T_0 \tag{24}$$

Boundary conditions in dimensionless form are:

$$u(\eta,z,t) = w(\eta,z,t) = 0,\ T(\eta,z,t) = T_w \quad \text{on } \eta = 1 \tag{25}$$

$$\frac{\partial w(\eta,z,t)}{\partial \eta} = 0, \ \frac{\partial T(\eta,z,t)}{\partial \eta} = 0\,, \ u(\eta,z,t) = 0 \quad \text{on} \quad \eta = 0 \tag{26}$$

Since z_0 is the half-length of stenotic region and e is the height of stenosis, then the dimensionless state of the geometry of atherosclerotic artery takes, the form:

$$h(z) = \begin{cases} 1 - e\big(1 + cos(\pi z)\big) & for\ -1 < z \leq 1 \\ 1 & \text{otherwise.} \end{cases}$$

Solution of Mathematical Model Equations

To obtain the solution of the problem, first, the constricted part of the arterial segment is transformed from a cylindrical domain with a varying boundary (due to constriction) to a rectangular domain with a fixed boundary by introducing a new variable $\frac{\eta}{h(z)}$.

This approach offers several advantages in simplifying and solving the mathematical model formulated in case of geometric simplification, similarity scaling and normalizing radial coordinate system.

Therefore, under this transformation the new form of equations (15) – (18) leads to:

$$\frac{1}{h}\frac{\partial u}{\partial \chi} + \frac{u}{h\chi} + \frac{\partial w}{\partial z} - \frac{\chi}{h}\frac{dh}{dz}\frac{\partial w}{\partial \chi} = 0 \tag{27}$$

$$\frac{\partial u}{\partial t} = -\frac{u}{h}\frac{\partial u}{\partial \chi} - w\left(\frac{\partial u}{\partial z} - \frac{\chi}{h}\frac{dh}{dz}\frac{\partial u}{\partial \chi}\right) + \frac{1}{h}\frac{\partial \tau_{\chi\chi}}{\partial \chi} + \frac{\tau_{\chi\chi}}{h\chi} + \frac{\partial \tau_{\chi z}}{\partial z} - \frac{\chi}{h}\frac{dh}{dz}\frac{\partial \tau_{\chi z}}{\partial \chi} \tag{28}$$

$$\frac{\partial w}{\partial t} = A_0 + A_1 cos(\omega t) - \frac{u}{h}\frac{\partial w}{\partial \chi} - w\left(\frac{\partial w}{\partial z} - \frac{\chi}{h}\frac{dh}{dz}\frac{\partial w}{\partial \chi}\right) + \frac{1}{h}\frac{\partial \tau_{\chi z}}{\partial \chi} + \frac{\tau_{\chi z}}{h\chi} + \frac{\partial \tau_{zz}}{\partial z} - \frac{\chi}{h}\frac{dh}{dz}\frac{\partial \tau_{zz}}{\partial \chi} + a_0 \cos(\omega_1 t + \phi) - \frac{Ha^2}{Re} w \tag{29}$$

$$\frac{\partial T}{\partial t} = -\frac{u}{h}\frac{\partial T}{\partial \chi} - w\left(\frac{\partial T}{\partial z} - \frac{\chi}{h}\frac{dh}{dz}\frac{\partial T}{\partial \chi}\right) + \frac{1}{P_r}\left(\frac{1}{h^2}\frac{\partial^2 T}{\partial \chi^2} + \frac{1}{h^2\chi}\frac{\partial T}{\partial \chi} + \frac{\partial^2 T}{\partial z^2}\right) + \frac{1}{P_r}\left[\frac{2\chi}{h^2}\left(\frac{dh}{dz}\right)^2\frac{\partial T}{\partial \chi} - \frac{2\chi}{h}\frac{dh}{dz}\frac{\partial^2 T}{\partial \chi \partial z} - \frac{\chi}{h}\frac{\partial^2 h}{\partial z^2}\frac{\partial T}{\partial \chi} + 3\left(\frac{\chi}{h}\frac{dh}{dz}\right)^2\frac{\partial^2 T}{\partial \chi^2}\right] + Ec\left[\frac{\tau_{\chi\chi}}{h}\frac{\partial u}{\partial \chi} + \tau_{\chi z}\left(\frac{\partial w}{h\partial \chi} + \frac{\partial u}{\partial z} - \frac{\chi}{h}\frac{dh}{dz}\frac{\partial u}{\partial \chi}\right) + \tau_{zz}\left(\frac{\partial w}{\partial z} - \frac{\chi}{h}\frac{dh}{dz}\frac{\partial w}{\partial \chi}\right)\right] + RdT \tag{30}$$

Where by:

$$\tau_{\chi\chi} = 2\left(\frac{1}{Re}\dot{\Upsilon}^{n-1} + \tau_0\dot{\Upsilon}^{-1}\right)\frac{\partial u}{h\partial \chi} \tag{31}$$

$$\tau_{zz} = 2\left(\frac{1}{Re}\dot{\Upsilon}^{n-1} + \tau_0\dot{\Upsilon}^{-1}\right)\left(\frac{\partial w}{\partial z} - \frac{\chi}{h}\frac{dh}{dz}\frac{\partial w}{\partial \chi}\right) \tag{32}$$

$$\tau_{\chi z} = \left(\frac{1}{Re}\dot{\Upsilon}^{n-1} + \tau_0\dot{\Upsilon}^{-1}\right)\left(\frac{\partial u}{\partial z} - \frac{\chi}{h}\frac{dh}{dz}\frac{\partial u}{\partial \chi} + \frac{1}{h}\frac{\partial w}{\partial \chi}\right) \tag{33}$$

with

$$\dot{\Upsilon}^2 = 2\left[\left(\frac{\partial u}{h\partial \chi}\right)^2 + \left(\frac{u}{h\chi}\right)^2 + \left(\frac{\partial w}{\partial z} - \frac{\chi}{h}\frac{dh}{dz}\frac{\partial w}{\partial \chi}\right)^2\right] + \left(\frac{\partial u}{\partial z} - \frac{\chi}{h}\frac{dh}{dz}\frac{\partial u}{\partial \chi} + \frac{1}{h}\frac{\partial w}{\partial \chi}\right)^2 \tag{34}$$

The initial and boundary conditions after this radial transformation are;

$$u(\chi, z, 0) = 0, \quad w_0 = \left(\frac{A_0 + A_1}{4}\right)[1 - (h\chi)^2] \quad \text{and} \quad T(\chi, z, 0) = T_0 \tag{35}$$

$$u(\chi, z, t) = w(\chi, z, t) = 0, \ T(\chi, z, t) = T_w \quad \text{at} \quad \chi = 1 \tag{36}$$

$$\frac{\partial w(\chi,z,t)}{\partial \chi} = 0, \ \frac{\partial T(\chi,z,t)}{\partial \chi} = 0, \ u(\chi, z, t) = 0 \quad \text{at } \chi = 0 \tag{37}$$

Radial momentum transformation

In order to obtain the radial velocity component $u(\chi, z, t)$ the continuity equation (27) is multiplied by $h\chi$ and then integrated w.r.t χ to obtain equation (38) below

$$\int \left(\chi\frac{\partial u}{\partial \chi} + u + \chi h\frac{\partial w}{\partial z} - \chi^2\frac{dh}{dz}\frac{\partial w}{\partial \chi}\right)d\chi = 0 \tag{38}$$

Re-arranging equation (38) we obtain

$$\int \chi\frac{\partial u}{\partial \chi}d\chi + \int u d\chi = \int \chi^2\frac{dh}{dz}\frac{\partial w}{\partial \chi}d\chi - \int \chi h\frac{\partial w}{\partial z}d\chi \tag{39}$$

Performing integration by parts and simplifying equation (39) yield;

$$u = \frac{dh}{dz}\chi w - \frac{2}{\chi}\frac{dh}{dz}\int w\chi d\chi - \frac{h}{\chi}\int \chi\frac{\partial w}{\partial z}d\chi \tag{40}$$

Fixing the boundary conditions (36) and (37) into equation (40) leads to the re-arranged equation of the form;

$$\frac{2}{\chi}\frac{dh}{dz}\int_0^1 w\chi d\chi = -\frac{h}{\chi}\int_0^1 \chi\frac{\partial w}{\partial z}d\chi \tag{41}$$

Multiplying by $\frac{\chi}{h}$ both sides we get the equation

$$\frac{2}{h}\frac{dh}{dz}\int_0^1 w\chi d\chi = -\int_0^1 \chi\frac{\partial w}{\partial z}d\chi \tag{42}$$

This finally simplifies to:

$$u = \chi\frac{dh}{dz}w \tag{43}$$

The equation (43) represents the radial velocity component which is required to be computed.
Then, differentiating (43) by product rule w.r.t χ and z respectively yields:

$$\frac{\partial u}{\partial \chi} = w\frac{dh}{dz} + \chi\frac{dh}{dz}\frac{\partial w}{\partial \chi} \tag{44}$$

$$\frac{\partial u}{\partial z} = \chi\frac{dh}{dz}\frac{\partial w}{\partial z} + \chi\frac{d^2h}{dz^2}w \tag{45}$$

The equations (44) - (45) represent the transformation of radial velocity $\boldsymbol{u}$ to axial velocity $\boldsymbol{w}$ within the flow field. Now inserting these equations into axial momentum and energy equations in (29) and (30) respectively yields the continuous system of the model equations as follows:

$$\frac{\partial w}{\partial t} = A_0 + A_1\cos(\omega t) - w\frac{\partial w}{\partial z} + \frac{1}{h}\frac{\partial \tau_{\chi z}}{\partial \chi} + \frac{\tau_{\chi z}}{h\chi} + \frac{\partial \tau_{zz}}{\partial z} - \frac{\chi}{h}\frac{dh}{dz}\frac{\partial \tau_{zz}}{\partial \chi} + a_0\cos(\omega_1 t + \phi) - \frac{Ha^2}{Re}w \tag{46}$$

$$\frac{\partial T}{\partial t} = -w\frac{\partial T}{\partial z} + \frac{1}{P_r}\left(\frac{1}{h^2}\frac{\partial^2 T}{\partial \chi^2} + \frac{1}{h^2\chi}\frac{\partial T}{\partial \chi} + \frac{\partial^2 T}{\partial z^2}\right) + \frac{1}{P_r}\left[\frac{2\chi}{h^2}\left(\frac{dh}{dz}\right)^2\frac{\partial T}{\partial \chi} - \frac{2\chi}{h}\frac{dh}{dz}\frac{\partial^2 T}{\partial \chi \partial z} - \frac{\chi}{h}\frac{\partial^2 h}{\partial z^2}\frac{\partial T}{\partial \chi} + 3\left(\frac{\chi}{h}\frac{dh}{dz}\right)^2\frac{\partial^2 T}{\partial \chi^2}\right] + Ec\left[\frac{\tau_{\chi\chi}}{h}\frac{dh}{dz}\left(w + \chi\frac{\partial w}{\partial \chi}\right) + \frac{\tau_{\chi z}}{h}\frac{\partial w}{\partial \chi}\right] + Ec\tau_{\chi z}\left[\chi\left(\frac{dh}{dz}\frac{\partial w}{\partial z} + w\frac{d^2h}{dz^2}\right)\right] - Ec\tau_{\chi z}\left[\frac{\chi}{h}\left(\frac{dh}{dz}\right)^2\left(w + \chi\frac{\partial w}{\partial \chi}\right)\right] + Ec\tau_{zz}\left(\frac{\partial w}{\partial z} - \frac{\chi}{h}\frac{dh}{dz}\frac{\partial w}{\partial \chi}\right) + RdT \tag{47}$$

with

$$\dot{\Upsilon} = \sqrt{2\left[\frac{dh}{hdz}\left(\chi\frac{\partial w}{\partial \chi} + w\right)^2 + \left(\frac{w}{h}\frac{dh}{dz}\right)^2 + \left(\frac{\partial w}{\partial z} - \frac{\chi}{h}\frac{dh}{dz}\frac{\partial w}{\partial \chi}\right)^2\right] + \left(\chi\left(\frac{dh}{dz}\frac{\partial w}{\partial z} + w\frac{d^2h}{dz^2}\right) - \frac{\chi}{h}\left(\frac{dh}{dz}\right)^2\left(\chi\frac{\partial w}{\partial \chi} + w\right) + \frac{\partial w}{h\partial \chi}\right)^2} \tag{48}$$

and

$$\tau_{\chi\chi} = 2\left(\frac{1}{Re}\dot{\Upsilon}^{n-1} + \tau_0\dot{\Upsilon}^{-1}\right)\frac{dh}{dz}\left(\chi\frac{\partial w}{\partial \chi} + w\right) \tag{49}$$

$$\tau_{zz} = 2\left(\frac{1}{Re}\dot{\Upsilon}^{n-1} + \tau_0\dot{\Upsilon}^{-1}\right)\left(\frac{\partial w}{\partial z} - \frac{\chi}{h}\frac{dh}{dz}\frac{\partial w}{\partial \chi}\right) \tag{50}$$

$$\tau_{\chi z} = \left(\frac{1}{Re}\dot{\Upsilon}^{n-1} + \tau_0\dot{\Upsilon}^{-1}\right)\left[\chi\left(\frac{dh}{dz}\frac{\partial w}{\partial z} + w\frac{d^2h}{dz^2}\right) - \frac{\chi}{h}\left(\frac{dh}{dz}\right)^2\left(\chi\frac{\partial w}{\partial \chi} + w\right) + \frac{\partial w}{h\partial \chi}\right] \tag{51}$$

Numerical discretization of the Dimensionless Equations

The discretization process of the continuous model equations (46) - (47) to a discrete system of algebraic equations is shown as follows: The Finite difference method (FDM) is involved to solve the discrete model equations. This method is better in approximation of higher order derivatives which are useful in implementation of different fluid dynamics models. In favor of this, explicit FDM scheme is chosen and believed to produce the best possible approximate results of this study compared to others. The first order derivatives are replaced explicitly by the forward difference method and second order derivatives are discretized by the central difference method. The similar method was employed (among others) by (Mustapha and Amin (2008), Sharma and Gaur (2018), and Liu and Liu (2020)). The approximate derivatives are displayed below:

$$\frac{\partial w}{\partial \chi} = \frac{w_{i,j+1}^k - w_{i,j-1}^k}{2\Delta\chi},\ \frac{\partial^2 w}{\partial \chi^2} = \frac{w_{i,j+1}^k - 2w_{i,j}^k + w_{i,j-1}^k}{(\Delta\chi)^2},\ \frac{\partial w}{\partial t} = \frac{w_{i,j}^{k+1} - w_{i,j}^k}{\Delta t} \tag{52}$$

Similarly, the derivatives of $\boldsymbol{\tau_{\chi z}}$ and $\boldsymbol{\tau_{zz}}$ are also computed below.

$$\frac{\partial \tau_{\chi z}}{\partial \chi}=\frac{(\tau_{\chi z})^{k}_{i,j+1}-(\tau_{\chi z})^{k}_{i,j-1}}{2\Delta\chi},\frac{\partial \tau_{zz}}{\partial \chi}=\frac{(\tau_{zz})^{k}_{i,j+1}-(\tau_{zz})^{k}_{i,j-1}}{2\Delta\chi},\frac{\partial \tau_{zz}}{\partial z}=\frac{(\tau_{zz})^{k}_{i+1,j}-(\tau_{zz})^{k}_{i-1,j}}{2\Delta z} \tag{53}$$

Also, it is further defined that:

$$\begin{cases}\chi_j=(j-1)\Delta\chi; & j=1,2,3\ldots\ldots(N+1) \quad \text{for which} \quad \chi_{N+1}=1\\ z_i=(i-1)\Delta z; & \text{for} \quad i=1,2,3\ldots\ldots(M+1)\\ t_k=(k-1)\Delta t; & \text{for} \quad k=1,2,3\ldots\ldots\ldots\ldots\end{cases} \tag{54}$$

Therefore, the substitution of equations (52) – (54) into (46) – (47) is done by making $\boldsymbol{w}$ and $\boldsymbol{T}$ the subject and if the radial velocity discretization is also done, then the final system of discrete equations is displayed in the following way:

$$u^{k+1}_{i,j}=\chi_j\left(\frac{dh}{dz}\right)_i w^{k}_{i,j} \tag{55}$$

$$\begin{aligned}(w)^{k+1}_{i,j}=w^{k}_{i,j}+\Delta t\left(A_0+A_1cos(\omega t)+a_0\cos(\omega_1 t+\phi)-\frac{Ha^2}{Re}w^{k}_{i,j}\right)-\\ \Delta t\left[w^{k}_{i,j}\left(\frac{w^{k}_{i+1,j}-w^{k}_{i-1,j}}{2\Delta z}\right)+\frac{\chi_j}{h_i}\left(\frac{dh}{dz}\right)_i\left(\frac{(\tau_{zz})^{k}_{i,j+1}-(\tau_{zz})^{k}_{i,j-1}}{2\Delta\chi}\right)\right]+\\ \Delta t\left[\frac{1}{h_i}\left(\frac{(\tau_{\chi z})^{k}_{i,j+1}-(\tau_{\chi z})^{k}_{i,j-1}}{2\Delta\chi}\right)+\frac{(\tau_{\chi z})^{k}_{i,j}}{h_i\chi_j}+\left(\frac{(\tau_{zz})^{k}_{i+1,j}-(\tau_{zz})^{k}_{i-1,j}}{2\Delta z}\right)\right]\end{aligned} \tag{56}$$

$$\begin{aligned}T^{k+1}_{i,j}=T^{k}_{i,j}-\Delta t\left(w^{k}_{i,j}\left(\frac{T^{k}_{i+1,j}-T^{k}_{i-1,j}}{2\Delta z}\right)\right)+\frac{\Delta t}{P_r}\left[\frac{T^{k}_{i,j+1}-2T^{k}_{i,j}+T^{k}_{i,j-1}}{{h_i}^2(\Delta\chi)^2}+\frac{T^{k}_{i,j+1}-T^{k}_{i,j-1}}{2\chi_j{h_i}^2\Delta\chi}+\frac{T^{k}_{i+1,j}-2T^{k}_{i,j}+T^{k}_{i-1,j}}{(\Delta z)^2}\right]+\\ \frac{\Delta t}{P_r}\left[\frac{2\chi_j}{{h_i}^2}\left(\frac{dh}{dz}\right)^2_i\left(\frac{T^{k}_{i,j+1}-T^{k}_{i,j-1}}{2\Delta\chi}\right)-2\frac{\chi_j}{h_i}\left(\frac{dh}{dz}\right)_i\left(\frac{T^{k}_{i+1,j+1}-T^{k}_{i-1,j+1}+T^{k}_{i+1,j-1}+T^{k}_{i-1,j-1}}{4\Delta\chi\Delta z}\right)-\right.\\ \left.\frac{\chi_j}{h_i}\left(\frac{d^2h}{dz^2}\right)_i\left(\frac{T^{k}_{i,j+1}-T^{k}_{i,j-1}}{2\Delta\chi}\right)+3\left(\frac{\chi_j}{h_i}\frac{dh}{dz}\right)^2_i\left(\frac{T^{k}_{i,j+1}-2T^{k}_{i,j}+T^{k}_{i,j-1}}{(\Delta\chi)^2}\right)\right]+\\ \Delta tEc\left[\frac{(\tau_{\chi\chi})^{k}_{i,j}}{h_i}\left(\frac{dh}{dz}\right)_i\left(\chi_j\left(\frac{w^{k}_{i,j+1}-w^{k}_{i,j-1}}{2\Delta\chi}\right)+w^{k}_{i,j}\right)+\frac{(\tau_{\chi z})^{k}_{i,j}}{h_i}\left(\frac{w^{k}_{i,j+1}-w^{k}_{i,j-1}}{2\Delta\chi}\right)\right]\\ +\Delta tEc(\tau_{\chi z})^{k}_{i,j}\chi_j\left[\left(\frac{dh}{dz}\right)_i\left(\frac{w^{k}{}_{i+1,j}-w^{k}{}_{i-1,j}}{2\Delta z}\right)+w^{k}{}_{i,j}\left(\frac{d^2h}{dz^2}\right)_i\right]\\ -\Delta tEc(\tau_{\chi z})^{k}_{i,j}\frac{\chi_j}{h_i}\left(\frac{dh}{dz}\right)^2_i\left(\chi_j\left(\frac{w^{k}_{i,j+1}-w^{k}_{i,j-1}}{2\Delta\chi}\right)+w^{k}_{i,j}\right)\\ +\Delta tEc(\tau_{zz})^{k}_{i,j}\left[\left(\frac{w^{k}{}_{i+1,j}-w^{k}{}_{i-1,j}}{2\Delta z}\right)-\frac{\chi_j}{h_i}\left(\frac{dh}{dz}\right)_i\left(\frac{w^{k}_{i,j+1}-w^{k}_{i,j-1}}{2\Delta\chi}\right)\right]\\ +\Delta tEcRd\end{aligned} \tag{57}$$

with

$$\dot{\Upsilon}=\sqrt{\begin{aligned}&2\left[\left(\frac{1}{h_i}\left(\frac{dh}{dz}\right)_i\left(\chi_j\left(\frac{w^{k}_{i,j+1}-w^{k}_{i,j-1}}{2\Delta\chi}\right)+w^{k}_{i,j}\right)\right)^2+\left(\frac{1}{h_i}\left(\frac{dh}{dz}\right)_i w^{k}_{i,j}\right)^2\right]\\ &+2\left(\left(\frac{w^{k}_{i+1,j}-w^{k}_{i-1,j}}{2\Delta z}\right)-\frac{\chi_j}{h_i}\left(\frac{dh}{dz}\right)_i\left(\frac{w^{k}_{i,j+1}-w^{k}_{i,j-1}}{2\Delta\chi}\right)\right)^2+\left(\xi^{k}{}_{i,j}\right)^2\end{aligned}} \tag{58}$$

whereby

$$\xi^{k}{}_{i,j}=\chi_j\left(\frac{dh}{dz}\right)_i\left(\frac{w^{k}_{i+1,j}-w^{k}_{i-1,j}}{2\Delta z}\right)+w^{k}_{i,j}\left(\frac{d^2h}{dz^2}\right)_i-\frac{\chi_j}{h_i}\left(\frac{dh}{dz}\right)^2_i\left(\chi_j\left(\frac{w^{k}_{i,j+1}-w^{k}_{i,j-1}}{2\Delta\chi}\right)+w^{k}_{i,j}\right)+\frac{1}{h_i}\left(\frac{w^{k}_{i,j+1}-w^{k}_{i,j-1}}{2\Delta\chi}\right) \tag{59}$$

and

$$(\tau_{\chi\chi})^{k}{}_{i,j}=2\left(\frac{1}{Re}\dot{\Upsilon}^{n-1}+\tau_0\dot{\Upsilon}^{-1}\right)\left(\frac{dh}{dz}\right)_i\left(\chi_j\left(\frac{w^{k}_{i,j+1}-w^{k}_{i,j-1}}{2\Delta\chi}\right)+w^{k}_{i,j}\right) \tag{60}$$

$$(\tau_{zz})^{k}_{i,j} = 2\left(\frac{1}{Re}\dot{\Upsilon}^{n-1} + \tau_0\dot{\Upsilon}^{-1}\right)\left[\left(\frac{w^{k}_{i+1,j}-w^{k}_{i-1,j}}{2\Delta z}\right) - \frac{\chi_j}{h_i}\left(\frac{dh}{dz}\right)_i\left(\frac{w^{k}_{i,j+1}-w^{k}_{i,j-1}}{2\Delta\chi}\right)\right] \tag{61}$$

$$(\tau_{\chi z})^{k}_{i,j} = \left(\frac{1}{Re}\dot{\Upsilon}^{n-1} + \tau_0\dot{\Upsilon}^{-1}\right)\left[\chi_j\left(\frac{dh}{dz}\right)_i\left(\frac{w^{k}_{i+1,j}-w^{k}_{i-1,j}}{2\Delta z}\right) + w^{k}_{i,j}\left(\frac{d^2h}{dz^2}\right)_i + \frac{1}{h_i}\left(\frac{w^{k}_{i,j+1}-w^{k}_{i,j-1}}{2\Delta\chi}\right)\right] - \frac{\chi_j}{h_i}\left(\frac{dh}{dz}\right)^2_i\left(\chi_j\left(\frac{w^{k}_{i,j+1}-w^{k}_{i,j-1}}{2\Delta\chi}\right) + w^{k}_{i,j}\right) \tag{62}$$

The respective discretized boundary conditions are:

$$w_0 = w^{1}_{i,j},\ T^{1}_{i,j} = T_0,\ u^{1}_{i,j} = 0,\ w^{k}_{i,1} = u^{k}_{i,1} = 0 \tag{63}$$

$$w^{k}_{i,2} = w^{k}_{i,1},\ T^{k}_{i,2} = T^{k}_{i,1},\ w^{k}_{i,N+1} = u^{k}_{i,N+1} = (\tau_{\chi z})^{k}_{i,1} = 0,\ T^{k}_{i,N+1} = T_w \tag{64}$$

Results and Discussion

The numerical results of discretized equations (55) – (62) are here presented. The simulation process is done by MATLAB software, taken into the assumption of varying the following dimensionless parameters with their numerical values shown in the result plots:

Fixed Parameter	A_o	A_1	ω	ω_1	ϕ	Z_o	K	$\Delta\chi$	Δt	Δz
Value	1	0.8	1	1	0.3	0.5	0.2	0.04	0.01	0.1
Varying Parameter	Re	a_o	Ha	n	Ec	τ_o	Rd	Pr		
Values	1,2,3	1,3,5	1,2,3	0.69,0.95,1.6	1,3,5	0.1,0.3,0.5	0.1,0.8,1.5	21, 25, 28		

Some of these parameter values were obtained from existing literatures and others were assumed within realistic and physically meaningful ranges. In order to satisfy the geometry of the flow field stated earlier in equation (5), the domain interval for radial distance will range in $0 \le \chi \le 0.8$ and time derivative lies in $0 \le t \le 1$. The results are here displayed;

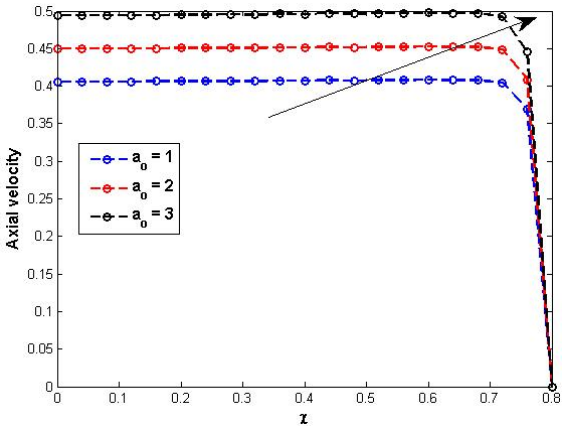

Figure 2: Effects of varying body acceleration on blood's axial velocity

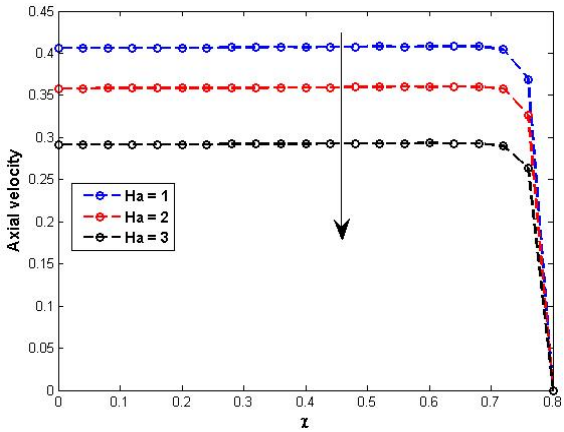

Figure 3: Increasing Hartman number on blood's axial velocity field.

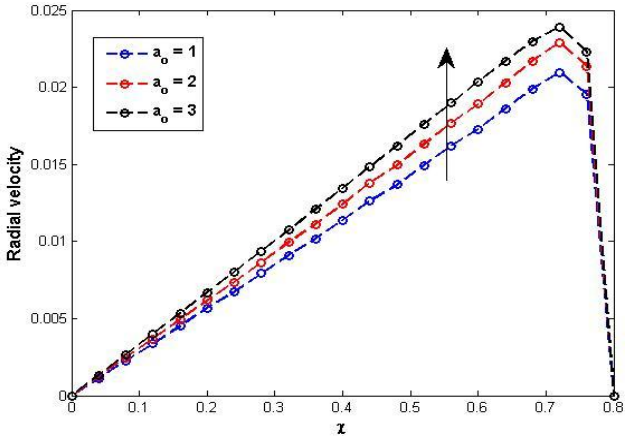

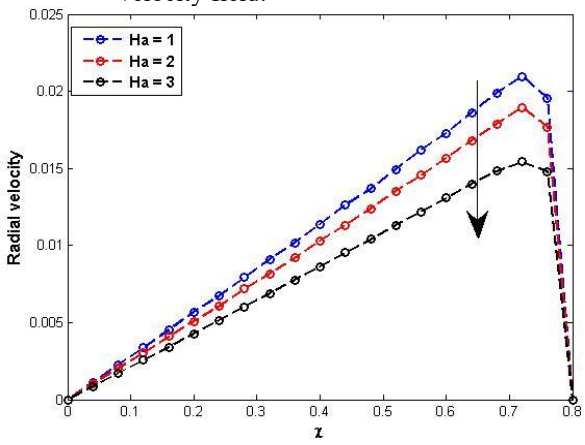

Figure 4: Varying body acceleration parameter on blood's radial velocity field

Figure 5: Increasing of Hartman number on blood' s radial velocity

Figure 2, identifies the effects of varying body acceleration parameter on axial velocity. The increase in body acceleration increases the velocity of blood and that is because whenever someone is subjected to hard physical exercises there occurs rapid increase of heartbeats and pulse rates. This results to increase in blood pressure enabling the rapid flow of blood from the heart towards the arterial regions of low pressure. This significantly rises blood velocity in arteries with low pressure. Similar results in discussion were done by (Tanwar et al. 2016 and Mwapinga et al. 2020). The variations of Hartman number on axial velocity were displayed in Figure 3. It was observed that the increase of Hartman number declines the velocity of blood. This results from the enhanced Lorentz force which retards the blood motion in the constricted artery (Varshiney et al. 2010). Furthermore, Figures 3 and 4, illustrate the effects of varying body acceleration and Hartman number on blood's radial velocity profile, in which their results coincide with what was observed in Figures 2 and 3.

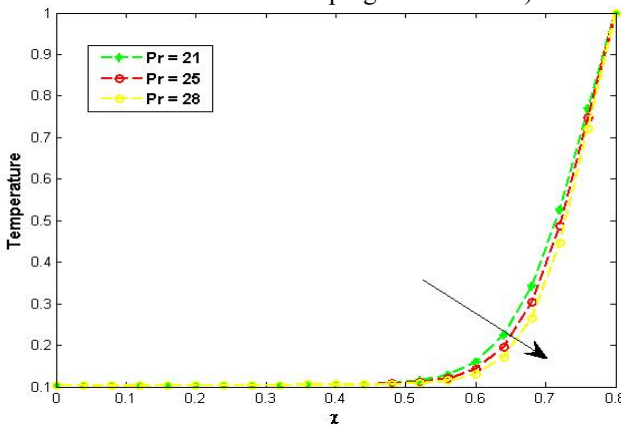

Figure 6: Increasing Prandtl number (***Pr***) on blood temperature profile

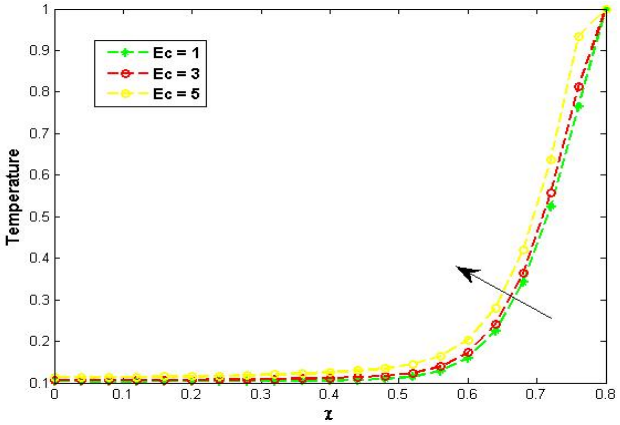

Figure 7: Effects of increasing Eckert (E_c) number on blood temperature

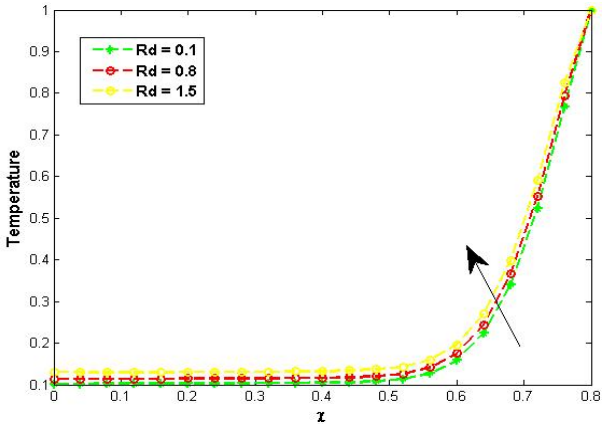

Figure 8: Effects of variation of radiation parameter source (***Rd***) on temperature profile

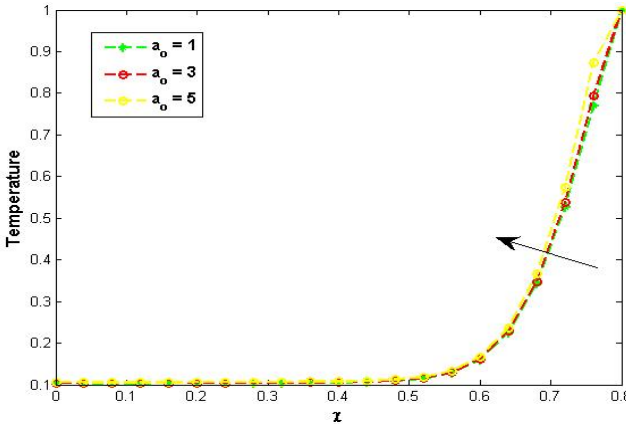

Figure 9: Effects of increasing body acceleration on blood's temperature profile

Figure 6, displays the effects of variations of Prandtl number on blood temperature. It is observed that the increase in Prandtl number reduces the temperature profile of the blood in the arterial segment. This is because if the blood attains high Prandtl number physically implies that its thermal diffusivity falls while its momentum diffusivity dominates the thermal boundary layer of the arterial wall. Figure 7, explores that the increase of Eckert number increases the temperature distribution in the blood. The Eckert number represents the amount of heat generated from friction of layers of blood due to relative motion. Thus, as the difference in temperature $T_w - T_0$ in the arterial geometry decreases the Eckert number becomes huge as a result heat emerges to flow from the blood layers to the arterial wall. Thus, this reinforces the coefficient of specific heat capacity of blood leading to increase in its temperature. These observations align with Sharma and Gaur, (2018) findings.

Figures 8-9, illustrate the results of variation of radiation parameter and body acceleration on the temperature profile respectively. These indicate that the increase of radiation parameter source in the blood system increase the temperature of the blood. This is due to fact that the presence of radiant energy in the arterial wall influences the improvement of surface heat flux in the arterial system. This offers the regulation of blood flow's resistance for proper circulation of hemoglobin to different parts of the body as it was explored by Zigta B, (2020). Consequently, the increase of body acceleration parameter enhances the

increase of core body temperature which eventually rises the blood temperature in the artery.

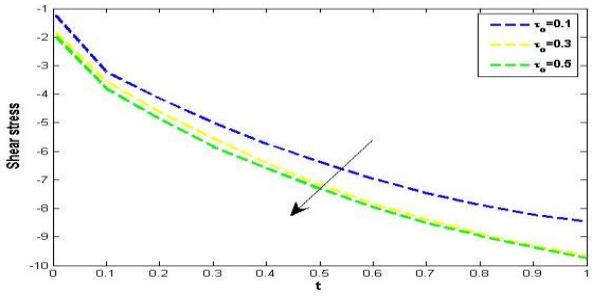

Figure 10: Varying yield stress (τ_0) on shear stress profile.

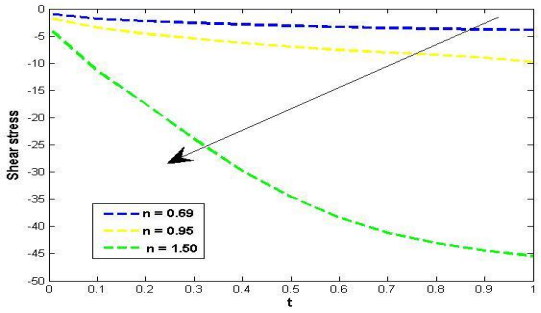

Figure.11: Effects of increasing flow index number (n) on shear stress profile

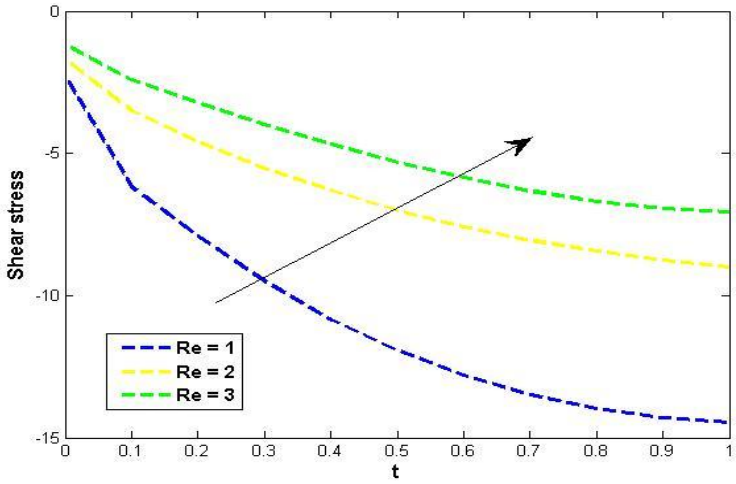

Figure 12: Variation of Reynolds' number (Re) on the shear stress

The variation of wall shear stresses is presented in Figures 12-14.

In Figures 10 and 11, it is observed that the magnitude of shear stress at the arterial wall increases as the yield stress and flow index number of blood increase. This implies that any amount of yield stress needed by the blood to flow offers a certain amount of shear stress at the stenosis throat which eventually decreases the blood flow rate. On the other hand, the increase in flow index number of the blood increases the thickness of blood to flow and hence yields higher shear stress at the wall of the stenosis region which also decreases the blood flow rate too. However, as the power index value $n > 1$ the shear stress increases towards large negative numbers physically enhancing the blood's viscosity in the narrowed artery (Mwapinga et al. 2020). This consequently offers higher resistance in the blood leading to downing the blood flow rate.

Figure 12, elaborates the effects of increasing generalized Reynolds number on shear stress. It is noted that the increase in Reynolds number of the blood diminishes the amount of shear stress in the arterial wall toward zero. This is because, the increase in Reynolds number lowers the consistency index of the blood K as the result, and the magnitude of stress is reduced toward zero. Physically, the increased Reynolds number enhances higher movement of blood molecules due to the decreased shear stress at the wall resulting to high blood flow rate in the arterial system. Similarly, the same findings were revealed by Liu and Liu, (2020).

Conclusion

The mathematical analysis of blood flow through an atherosclerotic artery using the Herschel-Bulkley non-Newtonian fluid model has displayed significant impacts of body acceleration, thermal radiation, and magnetic field effects on velocity, temperature, and shear stress profiles.

The results indicate that increasing body acceleration leads to a notable enhancement in both axial velocity and temperature of the blood. This behavior is attributed with the inertial effects introduced in the momentum and energy equations, which in turn promote a thicker velocity and thermal boundary layer.

In contrast, the presence of an applied transverse magnetic field introduces a Lorentz force that opposes the motion of blood, effectively reducing the axial velocity. This magnetic damping effect is clearly represented in the reduced velocity profile obtained from the numerical solutions of the momentum equation by increasing values of the Hartmann number.

Thermal radiation, incorporated via the Roseland approximation (radiative heat flux) in the energy equation, presents a direct correlation with the increase in blood temperature. Higher radiation parameters lead to an elevated thermal boundary layer thickness, which is evident from the enhanced temperature profiles across the arterial wall.

The parametric analysis further reveals that an increase in the flow behavior index n and yield stress τ_0 elevates the resistance to flow, consistent with the rheological behavior of the Herschel-Bulkley fluid model. These parameters increase the nonlinearity of the shear stress, reducing overall flow rate, as observed in the shear stress profiles. Additionally, an increase in the Reynolds number leads to a reduction in the consistency index K, implying a shear-thinning behavior that supports an increase in blood flow rate. The inverse relationship between $\Re$and wall shear stress cements the role of inertial effects in modulating thermodynamic resistance in stenosed arteries.

Therefore, since the applied magnetic field significantly reduces blood velocity via the Lorentz force, it is recommended that magnetic field intensity should be carefully optimized in therapeutic applications. Moreover, the moderate increase in body acceleration enhances both blood velocity and temperature profiles, indicating that controlled movement or body positioning may improve hemodynamic performance. Although, these effects should be quantified for individual cases using patient-specific parameters. Finally, the inclusion of thermal radiation in the model promotes blood temperature and thermal boundary layer thickness. This suggests a potential use of controlled thermal radiation (e.g. infrared therapies or thermotherapy) to enhance nutrient transport, provided that it aligns with safety thresholds for tissue exposure of affected arteries.

References

Amos E, Omamoke E and Chinedu, N 2022 Chemical Reaction, Heat Source and Slip Effects on MHD Pulsatory Blood Flowing Past an Inclined Stenosed Artery Influenced by Body Acceleration. *Int. J. Math. Trend. Technol.* 68(1):1-23.

Aziz UA, Muhammad UK, Sohail N, Muhammad HS, Ameer A, Fehmi G and Ahmed MH 2023 Analysis of pulsatile blood flow through elliptical multi-stenosed inclined artery influenced by body acceleration. *Eng. Sci. Technol. Int. J.* 47(4):1 - 8.

Das K and Saha G 2009 Arterial MHD pulsatile flow of blood under periodic body acceleration. *Bull. Soc. Math. Banja Luka.* 16*: 21-42.*

Devendra K, Satyanarayana B, Rajesh K, Sanjeev K and Narendra D 2021 Application of heat source and chemical reaction in MHD blood flow through permeable bifurcated arteries with inclined magnetic field in tumor treatments. *Res. Appl. Math*. 10(2021):100151.

Gupta PK, Singh J, Rai KN 2013 A numerical study of heat transfer in tissues during hyperthermia. *Math. Comput. Model.* 57(5):1018-1037.

Huang C, Chai Z and Shi B 2013 Non-Newtonian Effect on Hemodynamic Characteristics of Blood Flow in Stented Cerebral Aneurysm. *Comm. Comput. Phys.* 13(3):916–928.

Issah I, Christian JE and Rabiu M 2024 MHD flow of blood-Based Hybrid Nanofluid through a stenosed artery with thermal radiation Effect. *Case Stud. Therm. Eng.* 59(2024):104418.

Lilian M, Joash K, Vincent B 2023 Effect of Viscous Dis sipation (Φ) on Temperature Distribution of Blood Plasma in Presence of a Magnetic Field. Appl. Math. 14: 602-611.

Liu Y and Liu W 2020 Blood flow analysis in tapered stenosed arteries with the influence of heat and mass transfer. *J. Appl. Math. Comput.* 63(9): 1-19.

Mustapha N and Amin N 2008 The unsteady power law blood flow through a multi-regular stenosed artery. *MATEMATIKA.* 24:187-198.

Mwapinga A, Mureith E, Makungu J and Verdiana M 2020 Non-Newtonian heat and mass transfer on MHD pulsatile flow of blood through stenosed artery in the presence of body acceleration. *Commun. Math. Biol. Neurosci.* 64(2020): 1-27.

Sharma M and Gaur RK 2018 Radiation effect on MHD blood flow through a tapered porous stenosed artery with thermal and mass diffusion. Int. J. Appl. Mech. Eng. 24(2): 411-423.

Sinha A, Misra J and Shit G 2016 Effect of heat transfer on unsteady MHD flow of blood in a permeable vessel in the presence of non-uniform heat source. *Alex. Eng. J.* 55(2016): 2023-2033.

Sochi T 2013 Newtonian Flow in Converging-Diverging Capillaries. *Int. J. Model. Simul. Sci. Comput.* 4(03): 350011.

Tanwar VK, Varshiney N and Agarwal R 2016 Effect of body acceleration on pulsatile blood flow through a catheterized artery. *Adv. Appl. Sci. Res.* **7**(2):155-166.

Varshiney G, Katiyar VK and Kumar S 2010 Effect of magnetic field on the blood flow in artery with multiple stenosis. *Int. J. Eng. Sci. Technol.* 2(2): 967-982.

World Health Organization 2025 Leading causes of death and disability worldwide: *https://www.who.int.* 2000-2019

Zigta B 2020 The Effect of Thermal Radiation and Chemical reaction on MHD flow of Blood in Stretched permeable vessel. *Int. J. Appl. Mech. Eng*. 25(3):198-211.